

Identification of Enhancing MS Lesions in MR Images using Non-Parametric Image Subtraction

P. A. Bromiley*, M. Pokric, and N.A. Thacker

Imaging Science and Biomedical Engineering, Stopford Building,
University of Manchester, Oxford Road, Manchester, M13 9PT.

Abstract. Simple pixel-by-pixel image subtraction is widely used in image analysis to identify changes in image pairs. For example, multiple sclerosis (MS) produces lesions in the brain that can be detected by subtraction of MRI scans taken before and after the injection of GdDTPA contrast agent, which highlights the lesions. However, the result is returned in arbitrary units of pixel grey-level, with no statistically well-defined meaning. We describe a new, non-parametric subtraction measure, analogous to standard statistical tests, which allows regional data fusion and direct probabilistic interpretation of image differences. We demonstrate the technique using scans of MS lesions, but is expected to be applicable to a wide range of image formation processes.

1 Introduction

Image subtraction is widely used to analyse differences between pairs of images. However, interpretation of the resulting difference image presents a range of difficulties [1]. Identification of changes between images through the application of a threshold to a simple subtraction result is equivalent to the formation of a null hypothesis test statistic, using the assumption of a single distribution for the expected level of change, due to uniform noise. Successful use of this technique therefore requires that the only differences between the image pair are due to the mechanisms of interest, and this may in turn require sophisticated realignment and pre-processing of the image pair to remove gross changes prior to subtraction. In addition, although the result can be used immediately to identify regions of maximal change, it is quoted in arbitrary units of grey-level with no statistically well-defined meaning. This obstructs any quantitative analysis of the results. Ultimately it would be desirable to obtain a quantitative, statistical interpretation of the significance of the changes. Generally no known statistical model of the image data, or perhaps even the imaging process, will be available. However, sufficient data is usually available in the image pair to extract a sensible model of data behaviour from the data itself. Non-parametric image subtraction [2] uses this approach to obtain quantitative, statistically well-defined measures of difference for arbitrary image pairs.

2 Method

Non-parametric image subtraction [2] measures the differences between a pair of images in terms of an implicit model of the data behaviour. This is obtained in the form of a scattergram $S(g_1, g_2)$ of the grey levels g_1, g_2 of pairs of pixels at corresponding positions in the two images. A vertical slice in the scattergram isolates all pixels in image 1 with some grey level $g_1 = \text{const}$. The distribution of this data $G(g_1 = \text{const}, g_2)$ gives the relative frequency of grey levels for the corresponding pixels in the other image. Normalisation converts these frequencies into probabilities. An integration is then performed along the vertical slice passing through the coordinates defined by each pixel pair, summing all smaller probabilities. This is directly equivalent to the construction of a confidence interval [3], giving the probability of finding a more uncommon pairing of grey-levels than that seen at the original pixel pair. This probability can then be used to produce a statistical difference map. Since the probability is calculated with reference to the data itself, only localised (rather than global) differences between the images will be detected. In addition, the technique is asymmetric under interchange of data, so only localised differences in the image plotted on the ordinate of the scattergram will be identified.

The technique is based on a probability integral transform, so the distribution of grey levels in the difference image is by definition uniform (and therefore honest), providing a mechanism for self-test. In addition the equation [4],

$$F_n(p) = p \sum_{j=0}^{n-1} \frac{(-\ln p)^j}{j!} \quad \text{where } p = \prod_i^n \omega_i, \quad (1)$$

exists to renormalise any quantity p that is the product of n independent quantities ω_i , each drawn from a uniform probability distribution, such that $F_n(p)$ also has a uniform distribution. A derivation for this equation is given

* E-mail: paul.bromiley@talk21.com

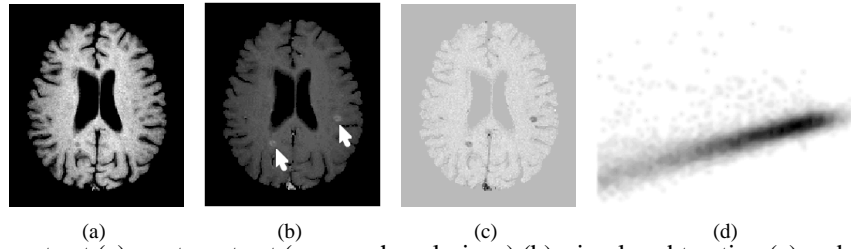


Figure 1. Pre-contrast (a), post-contrast (arrows show lesions) (b), simple subtraction (c) and scattergram (d).

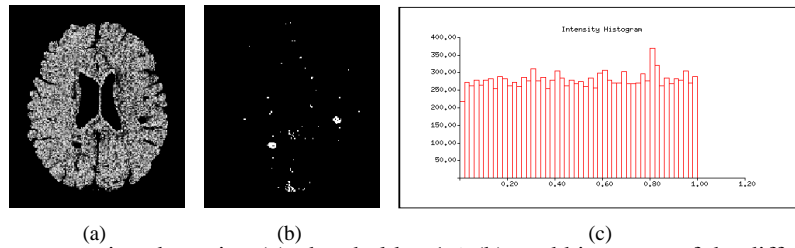


Figure 2. Non-parametric subtraction (a), threshold at 1% (b), and histogram of the difference image (c).

in [5]. This immediately provides a technique for refining the identification of localised differences between the images by forming the product of each pixel in the difference image with its four nearest neighbours. Statistically significant localised differences produce spatially correlated clusters of low-probability pixels in the difference image. They will therefore form low probability products that will not renormalise correctly. The effects of spatial correlation on the background pixels will produce a reduction in the effective number of degrees of freedom [6], which can be corrected by reducing the value of n used in Eqn. 1 using the non-integer generalisation of that equation in terms of gamma functions

$$F_n(p) = \frac{\Gamma(n, -\ln(p))}{\Gamma(n)} \quad \text{where } p = \prod_i^n \omega_i, \quad (2)$$

derived in Appendix A. ¹ The probability distribution for the renormalised products will then be uniform for background pixels, but will feature a spike close to zero for localised difference pixels. This spike can be extracted using thresholding, allowing automatic identification of the image differences.

3 Results

In order to demonstrate the applicability of the non-parametric image subtraction technique to identifying small but significant changes in medical images, whilst ignoring global differences such as those caused by repeat scanning over time or on different scanners, it was applied to the problem of MS lesion identification. Pre- and post-contrast T1 weighted images were obtained in a single patient at each of five visits. Visits were spaced approximately two months apart over a one-year period. Imaging consisted of contiguous 3mm T1 weighted spin echo images (TR/TE, 650/12, FOV 50mm², matrix 256²). The contrast agent injection consisted of 1mmols/kg of GdDTPA (Omniscan, Nycomed, Oslo, Norway). All volumes were co-registered to the pre-injection scans from the first visit, using the rigid co-registration software within Tina [7], and then re-sliced using normalised sinc interpolation with a 5x5x5 kernel to produce the co-registered volumes. Binary masks covering the brain (grey matter and white matter) were produced for these images, using a simple gradient-based segmentation technique. This allowed the subtraction to be performed only on the tissues of interest.

Fig. 1 shows pre- and post-contrast scans of a slice featuring two enhancing MS lesions, taken at the same visit, together with the result of simple subtraction and the scattergram for this image pair. Fig. 2 shows the result of the new subtraction technique applied to this image pair. The lesions (together with any other enhancing tissues, such as vasculature) are identified as regions of low-probabilities (dark regions) against a background of random noise

¹Selection of the required n can be made automatic by generating a flat reference histogram and comparing it to the histogram of the renormalised image using one of the standard goodness-of-fit tests, such as the Kolmogorov-Smirnov test or the χ^2 test, and performing a golden-section search on the value of n to find the best fit.

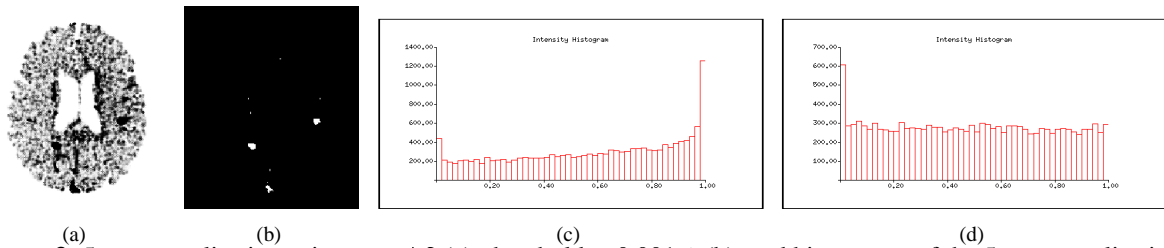


Figure 3. 5x renormalisation using $n = 4.3$ (a), threshold at 0.001% (b), and histograms of the 5x renormalisation images using $n = 5$ (c) and $n = 4.3$ (d).

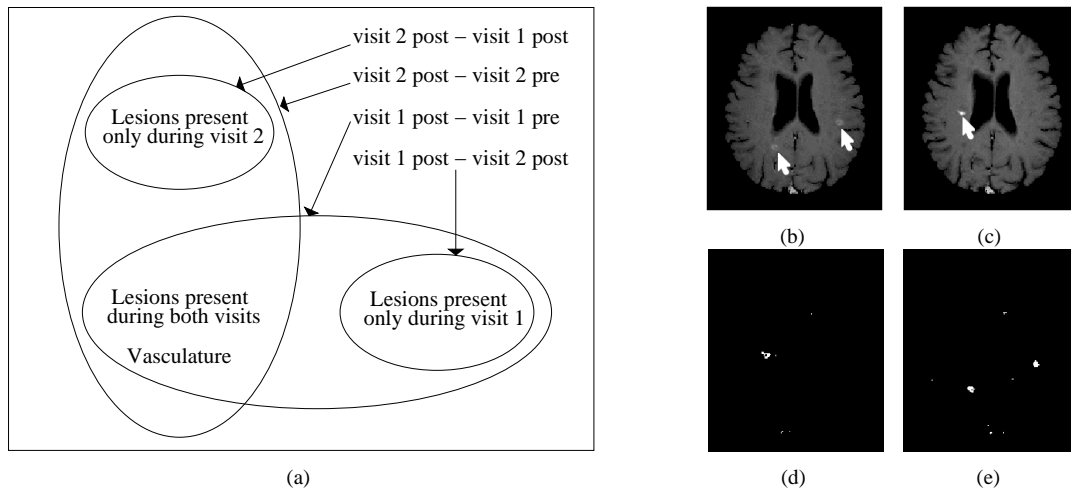


Figure 4. The groups of lesions identified by non-parametric subtractions between the four possible combinations of images from pre- and post-contrast scans taken during two visits (a). Post contrast scans from two visits (arrows show lesions) (b,c); 5x renormalised NPI subtraction c-b, thresholded at $1 \times 10^{-7}\%$ (d); same for b-c (e).

with a flat probability distribution. Since the result is quoted in terms of a probability, a statistically well-defined quantity subsequent analysis can be performed in a quantitative manner. As a simple example, Fig. 2b shows the result of applying a threshold to the difference image at the 1% level, extracting the lowest probability 1% of the pixels from the image. This identified tissues highlighted by the contrast agent, including both enhancing MS lesions and the vasculature. The identification of the lesions is clearly better than in the simple subtraction result (Fig. 1c). The histogram of the difference image (Fig. 2c) is flat, providing a self-test that demonstrates the applicability of the technique to this data.

Fig. 3 shows the result of applying the Eqn. 1 to the product of each pixel in the difference image with its four nearest neighbours (the “5x renormalisation”). This allows the lesions to be extracted at much lower thresholds (Fig. 3b), and so much of the background contamination due to vasculature is eliminated. The histogram of the product renormalised with $n = 5$ (Fig. 3c) is not flat, showing the reduction in the effective number of degrees of freedom due to the spatial correlation present in the difference image. This was corrected by reducing the value of n used to 4.3, producing a histogram with a flat distribution for background pixels (Fig. 3d).

Fig. 4 shows subtractions between post-contrast scans taken during visits separated by approximately two months. Subtractions between these scans identify changes in the enhancing tissues over time, rather than the enhancing tissues themselves. Furthermore, the asymmetry of the subtraction technique can be exploited to identify enhancing tissues present only in the second scan (Fig. 4d), or only in the first (Fig. 4e), simply by plotting these images on the ordinate of the scattergram. Fig. 4a shows the various combinations of images available. The 5x renormalisation technique described above has been applied to the results shown to further enhance lesion identification. These subtractions clearly show the changes in the lesions, again with some small contamination from vasculature.

4 Conclusions

The detection of MS lesions in MRI scans is an important issue both in relation to monitoring the progress of the pre-clinical disease and to therapeutic trials [8]. Currently the most popular technique used for this purpose is visual

inspection of the scans. We have presented a novel image subtraction routine based upon conventional statistical approaches that can identify small but significant differences between pairs of images in a robust manner, producing an output in terms of a probability. We have demonstrated the use of this measure in identification of MS lesions, and have shown it to be superior to simple subtraction. Unlike simple image subtraction, the new technique returns a result in terms of a probability, a statistically well-defined quantity, making quantitative analysis of the result a possibility. Such data can be used either directly or to focus partial volume analysis. We have also demonstrated that the technique can detect changes in enhancing lesions over time asymmetrically, for example showing only new enhancing lesions, providing a route to automatic measurement of disease progression. Finally, we have demonstrated a technique for refining the identification of enhancing lesions by analysing spatial correlation in the subtraction results. Although the examples given here relate to MS lesion identification, we expect the technique to be applicable to a wide range of image formation processes. A systematic study is now required to assess the use of this technique in clinical applications (e.g. prompting) and quantitative lesion studies.

Acknowledgments

The authors would like to acknowledge the support of the DTI Medilink Scheme grant no. P169 (Smart Inactivity Monitor using Array Based Detectors (SIMBAD)) in the development of the technique described here, and the support of Prof. Alan Jackson and the EPSRC and MRC (IRC: From Medical Images and Signals to Clinical Information) in obtaining the data used.

References

1. J. V. Hajnal, I. R. Young & G. M. Bidder. "Contrast mechanisms, functional MRI of the brain." In W. G. Bradley Jr. & G. Bydder (editors), *Advanced MR Imaging Techniques*, pp. 195–207. Martin Dunitz Ltd., London, 1997.
2. P. A. Bromiley, N. A. Thacker & P. Courtney. "Non-parametric image subtraction for MRI." In *Proceedings of MIUA 2001*, pp. 105–108. BMVA, 2001.
3. J. Neyman. "X-outline of a theory of statistical estimation based on the classical theory of probability." *Phil. Trans. Roy. Soc. Lond.* **A236**, pp. 333–380, 1937.
4. ALEPH Collaboration. "A precise measurement of $\gamma_{Z \rightarrow b\bar{b}}/\gamma_{Z \rightarrow hadrons}$." *Physics Letters* **B313**, pp. 535–548, 1993.
5. P. A. Bromiley, T. F. Cootes & N. A. Thacker. "Derivation of the renormalisation formula for the product of uniform probability distributions and extension to non-integer dimensionality." *TINA Memo 2001-008* 2001. Available from <http://www.tina-vision.net/docs/memos>.
6. K. Friston, P. Jezzard & R. Turner. "Analysis of functional mri time-series." *Human Brain Mapping* **1**, pp. 153–171, 1994.
7. N. A. Thacker, A. Lacey, E. Vorkurka et al. "TINA: an image analysis and computer vision application for medical imaging research." In *Proceedings of ECR 1999*, p. s556. Springer, 1999.
8. L. J. Wolansky, J. A. Bardini & S. D. Cook. "Triple-dose versus single dose gadoteridol in multiple sclerosis patients." *Journal of Neuroimaging* **4(3)**, pp. 141–145, 1994.

A Extension of the Renormalisation Equation to Non-Integer n

In order to generalise Eqn. 1 to non-integer values of n , it must be rewritten in terms of gamma functions. The complete gamma function $\Gamma(a)$ can be expressed as a sum of two functions called the upper and lower incomplete gamma functions, $\Gamma(a, z)$ and $\gamma(a, z)$ respectively, through

$$\Gamma(a) = (a-1)! = \int_0^\infty t^{a-1} e^{-t} dt = \int_0^z t^{a-1} e^{-t} dt + \int_z^\infty t^{a-1} e^{-t} dt = \gamma(a, z) + \Gamma(a, z) \quad (3)$$

$\gamma(a, z)$ has the series expansion

$$\gamma(a, z) = (a-1)! \left(1 - e^{-z} \sum_{i=0}^{a-1} \frac{z^i}{i!} \right) \quad (4)$$

Rearranging and using Eqn. 3 gives

$$\frac{\gamma(a, z)}{\Gamma(a)} = 1 - e^{-z} \sum_{i=0}^{a-1} \frac{z^i}{i!} \quad \text{so} \quad e^{-z} \sum_{i=0}^{a-1} \frac{z^i}{i!} = 1 - \frac{\gamma(a, z)}{\Gamma(a)} = \frac{\Gamma(a) - \gamma(a, z)}{\Gamma(a)} = \frac{\Gamma(a, z)}{\Gamma(a)} = Q(a, z) \quad (5)$$

The R.H.S. is also in common use, and is called the regularised upper incomplete gamma function $Q(a, z)$. Putting $a = n$ and $z = -\ln(p)$ gives the non-integer n generalisation of Eqn. 1

$$F_n(p) = p \sum_{j=0}^{n-1} \frac{(-\ln p)^j}{j!} = Q(n, -\ln(p)) \quad (6)$$